Int. J. Heat Mass Transfer. Vol. 36, No. 7, pp. 1727–1738, 1993
Printed in Great Britain

0017–9310/93 $6.00 + 0.00

The influence of the freezing process on vapour transport during sublimation in vacuum-freeze-drying of macroscopic samples

M. KOCHS,† CH. KÖRBER, I. HESCHEL and B. NUNNER
Helmholtz-Institut für Biomedizinische Technik an der RWTH Aachen, Pauwelsstraße 30, D-5100 Aachen, Germany

(*Received* 12 *July* 1991 *and in final form* 13 *July* 1992)

Abstract—The influence of freezing on mass transfer during subsequent sublimation was examined in macroscopic samples (cm scale). A matrix with regions of pure ice and regions of concentrated solution forms during freezing. In macroscopic samples, resulting from local differences in solidification conditions, this matrix is irregular, leading to local differences in mass transfer properties in the drying sample. A characteristic local distribution of diffusion coefficients in frozen, drying macroscopic samples could be analysed with differences amounting up to 425%. Sample segments at positions where solidification started yield small diffusion coefficients, the value increasing with the distance from this position, reaching a maximum in a layer right below the sample surface. A covering layer forms a limiting barrier against vapour transport. In macroscopic samples, a decrease of the applied cooling rate leads to a significant shift of the profile of space dependent diffusion coefficients to higher values and therefore to reduced drying times.

INTRODUCTION

FREEZE-DRYING is a preservation method which eliminates the water from an aqueous system at low temperatures. As the deteriorating effects of chemical and other reactions are slowed down or even stopped when water is removed, the product may be stored in the dry state for a long period at ambient temperature.

In general, freeze-drying consists of the following steps: freezing, primary and secondary drying, and rehydration. During freezing, the 'freezable' water undergoes a phase transition to ice. As most solutes are excluded from the ice, they are increasingly concentrated in the residual liquid. Resulting from the freezing procedure, there remains a matrix of ice and interstices, filled with concentrated solution, this solution being in a eutectic or amorphous state. Under the freezing methods normally applied in the freeze-drying process, the geometrical appearance of the forming ice crystals for the main part of the sample typically is that of columns, dendrites or 'ice fingers' [1, 2] (Fig. 1). As soon as the surface of the sample is exposed to a vacuum in the primary drying procedure, an ice–vapour interface begins to move through the specimen. The vapour sublimed at this interface is transported through the already ice-free part of the sample to the vacuum chamber. Mass transfer then is mainly performed through the void channels previously filled with ice (refs. [1–6]).

Hence the quality of all the succeeding steps of the freeze-drying process depends on the freezing process and the resulting texture in the sample.

In a companion paper [1], it was reported that there is a strong relationship between primary spacing λ_1 (i.e. the distance between the axes of symmetry of the ice fingers, Fig. 1) and the freezing parameters, i.e. interface velocity v_{il} and temperature gradient G at the ice–liquid interface. In a macroscopic sample, these parameters generally vary significantly in the course of the solidification process. For this reason, among others, the texture of a macroscopic sample usually changes with location. As a result of the local differences in texture, the mass transfer characteristics of a freeze-drying macroscopic sample also vary with position.

For a given product, an optimum thermal and chemical history during the freezing process (e.g. ref. [7]) and an ideal vapour pressure history leading to an optimum residual moisture content during drying (e.g. ref. [8]) can be observed, such that deteriorating effects are minimized. For designing an optimum freeze-drying cycle with respect to the requirements of the product, it is thus necessary to take into account the inhomogeneous freezing and drying conditions in a macroscopic sample.

In other experimental investigations on mass transfer in freeze-drying samples, an overall mass transfer coefficient for the already dry part of the sample was evaluated by measuring the weight loss during freeze-drying [4, 5, 9, 10] or by evaluating the mass flow through a freeze-dried sample with a pressure difference imposed on it [9, 11, 12].

In this paper, the mass transfer properties will be

† Presently at Pierburg GmbH, Alfred-Pierburg-Straße 1, D-4040 Neuss 1, Germany.

NOMENCLATURE

A cross sectional area of the sample perpendicular to the pressure gradient [m^2]

B_R cooling rate measured at the bottom of the sample [$K\,min^{-1}$]

D diffusion coefficient for vapour transport in a direction parallel to the axis of symmetry of the void channels of a freeze-drying sample in steady state measurements (cf. refs. [1, 2]) [$m^2\,s^{-1}$]

D_e effective diffusion coefficient for vapour transport through the void part of the sample ($x_{iv} < x < F$) related to the cross section of the sample perpendicular to the pressure gradient [$m^2\,s^{-1}$]

D_{ei} as D_e, the subscript 'i' indicating the number of the corresponding layer [$m^2\,s^{-1}$]

D_{en} as D_e, the subscript 'n' indicating, that D_{en} corresponds to the layer right in front of the interface [$m^2\,s^{-1}$]

D_{eo} effective overall diffusion coefficient for vapour transport through the void part of the sample [$m^2\,s^{-1}$]

D_K theoretical diffusion coefficient at molecular flow conditions [$m^2\,s^{-1}$]

F thickness of the frozen sample (here $F = 18.4$ mm) [m]

G mean tempeature gradient at the ice–liquid interface [$K\,m^{-1}$]

k_i thermal conductivity of ice [$W\,m^{-1}\,K^{-1}$]

k_s thermal conductivity of the frozen part of the sample (here the thermal conductivity of the solid was assumed to be an average value of the conductivities of the ice and the interstitial solution, weighted with their mass fractions in the solid, $k_s = 2.193\ W\,m^{-1}\,K^{-1}$) [$W\,m^{-1}\,K^{-1}$]

k_{H_2O} thermal conductivity of liquid water [$W\,m^{-1}\,K^{-1}$]

m mass of the sample [kg]

m_{tot} initial mass of the sample (here $m_{tot} = 22.3$ g) [kg]

M molecular weight [$kg\,kmol^{-1}$]

N_v mass flux of vapour through the void fraction of the sample, related to the total cross sectional area of the sample [$kg\,m^{-2}\,s^{-1}$]

p_{iv} vapour pressure at the ice–vapour interface [Pa]

p_v vapour pressure [Pa]

p_{vi} as p_v, the subscript 'i' indicating the number of the corrresponding layer [Pa]

p_∞ pressure in the drying chamber [Pa]

q heat flow through the ice-containing part of the sample [$W\,m^{-2}$]

r_e effective radius of the void capillaries [m]

r_s heat of sublimation [$J\,kg^{-1}$] (here $r_s\,(-26°C) = 2.892 \times 10^3\ kJ\,kg^{-1}$ [30]. With a maximum error of 0.8%, this value may be assumed as constant for the temperature range -36 to $-15°C$ which covers the experimental conditions (sublimation interface temperatures occurring in the experiments) [$J\,kg^{-1}$]

R_m universal gas constant [$J\,kmol^{-1}\,K^{-1}$]

R_v gas constant of vapour [$J\,kg^{-1}\,K^{-1}$]

R_{Di} resistance to vapour flow by a layer 'i' of the void part of the sample [$s\,m^{-1}$]

t time [s]

t_T drying time, i.e. time for the sublimation of 16 g of the ice, initially present in the sample [s]

T absolute temperature [K]

T_h temperature measured in the sample at the highest position [°C]

T_i initial temperature of the sample at the beginning of the freezing process [°C]

T_{iv} absolute temperature at the ice–vapour interface (it is assumed, that the dried part of the sample attains the temperature of the sublimation interface) [°C]

T_m temperature measured in the sample at the intermediate position [°C]

T_u temperature measured in the sample at the lowest position [°C]

T_R temperature at the bottom of the sample [°C]

v_{il} velocity of the ice–liquid interface [$m\,s^{-1}$]

x space coordinate, with origin at bottom of sample (Fig. 6) [m]

x_h position of the higher thermocouple [m]

x_{iv} position of the ice–vapour interface [m]

x_m position of the intermediate thermocouple [m]

x_u position of the lower thermocouple [m]

x_{un} mass fraction of the sample not undergoing the transformation to ice (solutes and 'bound water') (here $x_{un} = 0.142$, cf. ref. [41]) [-].

Greek symbols

λ_1 primary spacing, i.e. mean distance between neighbouring dendrites or cells ('ice fingers') [m]

ρ_v mass density of water vapour [$kg\,m^{-3}$].

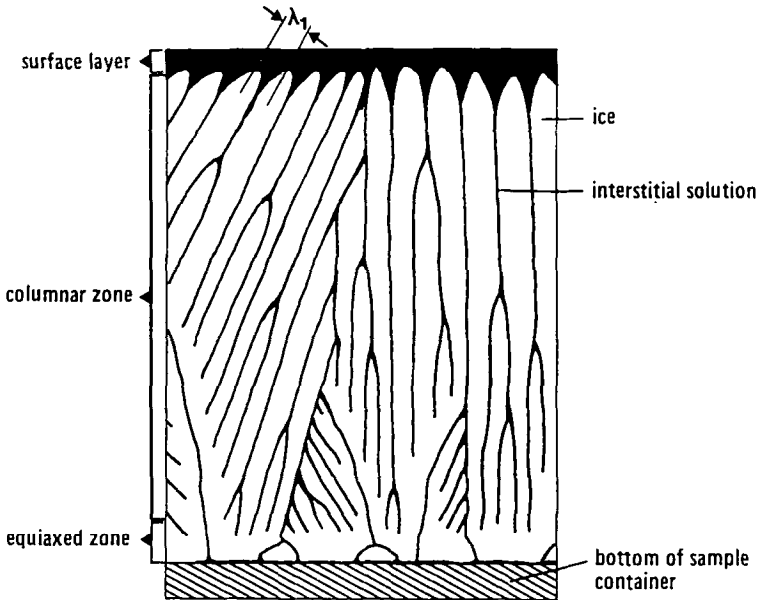

FIG. 1. Sketch of the inner texture of a frozen sample (partially redrawn from light-microscopic observations, cf. refs. [1, 2, 20, 22, 42]).

analysed separately for different layers of a macroscopic sample perpendicular to the heat and mass flow direction, and their dependence on the preceding freezing process will be investigated experimentally.

THEORETICAL CONSIDERATIONS

Cooling and freezing of a macroscopic sample

In the following it will be attempted to explain the dynamic freezing process in a macroscopic sample qualitatively (Fig. 1). As an example for the situation in a macroscopic sample, characteristic for many of the freeze-drying processes in use, the conditions in a freeze-drying tray filled with an aqueous solution are regarded. When a portion of the sample at sufficient distance from the side walls of the tray is considered, one-dimensional heat and mass transfer conditions may be assumed. The tray is usually placed on a shelf which is cooled to initiate solidification. A characteristic temperature profile forms inside the still liquid sample, with the coldest part being at the heat exchanging bottom of the sample. In this region the probability for the nucleation of ice is favoured compared to the rest of the sample: the temperature is lowest and thus the supercooling at this position reaches the highest values. For a given cooling rate, a higher supercooling causes a greater probability of the formation of homogeneous ice nuclei (e.g. ref. [13]). The probability of heterogeneous ice nucleation is highest at the bottom surface of the tray, where the wall material itself and possibly impurities sedimented onto it are present. After nucleation occurs at the bottom of the sample, a layer of equiaxed ice crystals grows very rapidly into the supercooled solution. The latent heat of crysallization is dissipated into the supercooled melt and into the container wall. Therefore, the temperature of the previously supercooled part of the sample and of the container wall is raised to the equilibrium freezing temperature of the sample solution [14] and the supercooling vanishes. The percentage of the sample undergoing this kind of equiaxed growth strongly depends on the degree of supercooling (the definition of 'equiaxed' chosen in this context is that the direction of crystal growth is the same as the heat flow direction, cf. ref. [15]). After this first stage of the solidification process, the ice crystals grow steadily towards the surface of the sample. The heat of crystallization is transported through the already frozen part of the specimen to the cooled bottom. Cellular or dendritic solidification occurs and a columnar, dendritic or 'finger-like' morphology of the interface results (cf. refs. [1, 2, 15]). The functional dependence of the primary spacing λ_1 from the parameters interface velocity v_{il} and temperature gradient G at the interface, $\lambda_1 \sim v^{-1/4} \cdot G^{-1/2}$ (cf. ref. [16, 17]), was confirmed experimentally for the dendritic solidification of an aqueous starch solution (10% wt hydroxyethyl starch in water) in Kochs *et al.* [1] for a steady state directional solidification process. The same type of starch solution is used in the bulk experiments described below. But, as steady state conditions usually do not occur in macroscopic samples, it has to be examined whether the results of steady state investigations are applicable for the prediction of the inner texture of parts of a macroscopic sample without correction. Studies on the dynamic development of the primary spacing λ_1 showed that especially in anisotropic systems (like

ice), the primary spacing only changes very slowly towards the steady state value when the solidification parameters (e.g. interface velocity v_{il}) are changed [18–21].

It may be concluded from the above, that there are two superimposed mechanisms influencing the morphology of the solidification interface and the texture after complete freezing in a macroscopic sample: the dynamic changing of the interface morphology (increase in λ_1) after the initial formation of the ice fingers out of equiaxed crystals and the dynamic change of the morphology due to the variation of the parameters v_{il} and G at the interface. A quantitative prediction of this texture is hardly possible to achieve. It is certain, however that the system always tends towards the steady state value of λ_1 so that an increase of the average values of v_{il} and G most probably will lead to a finer texture of the completely frozen sample.

The formation of a layer of highly concentrated solution on the surface of the sample is often observed in the macroscopic freezing of aqueous solutions [3, 9, 10, 22]. The development of this layer will be described in the following.

While the tips of the ice fingers grow towards the upper surface of the sample, the thickness of the ice fingers increases with the distance backwards from the tips. Due to the volume expansion during the transformation of water to ice, the material in the interstices between the ice fingers is expelled, effecting a convective flow of the highly concentrated solutes in these interstices towards the ice finger tips. Together with a diffusive mass transfer [23] from the regions of higher concentration into the still unsolidified part of the sample, the convective flow of concentrated solution towards the surface of the sample produces a macroscopic redistribution of the initially homogeneously distributed solutes. The effect of this redistribution in the main growth direction becomes most distinct when the ice finger tips approach the surface of the sample and the tip growth comes to an end. Then the flow of highly concentrated solutes out of the interstices produces a layer of concentrated solutes on the surface of the sample. The so-called macrosegregation in contrast to the mostly lateral microsegregation within the interdendritic channels (cf. refs. [15, 24]) was modelled and experimentally confirmed for the solidification of an aqueous NaCl solution in Jochem [25].

According to the considerations above, there are three regions in a completely frozen sample with distinct differences in morphology (cf. Fig. 1): a bottom layer with equiaxed crystals, a region with finger-shaped crystals (which covers the main part of the sample) and a surface layer of highly concentrated solution.

Mass transfer during sublimation

For sublimation, the free surface of the frozen sample is exposed to a vacuum. An ice–vapour interface begins to move from the surface towards the bottom of the sample. The vapour subliming at this interface has to be transported through the already ice-free part of the sample and the surface layer, which both form a resistance to vapour flow. The different resistances occurring during drying may be derived as a function of the above explained texture of a frozen sample (cf. Figs. 1 and 2).

The surface layer, consisting of highly concentrated solution, forms a significant barrier to the vapour flow [3, 9, 10, 12]. As long as no cracks [9, 26] are present in the sample, the vapour is transported in this layer with solid state diffusion. In the region where the ice crystals have the form of ice fingers, and where the vapour transfer is performed through the channels previously filled with ice, vapour transfer may be regarded as mass transfer through fine pores (the average diameter of the pores is assumed to be of the same order as the dendrite spacing, i.e. $\lambda_1 \approx 2 \cdot r_e$). For this case, the kinetic theory of gases provides equations for the diffusion coefficient [27] which are applicable (with small modifications) for the case of freeze-drying. This was confirmed for the case of Knudsen diffusion for the freeze-drying of an aqueous starch solution (cf. refs. [1, 2]).

As mentioned above, the primary spacing λ_1 varies with the position in a macroscopic sample due to the non-homogeneous freezing conditions. Thus the pore radius r_e also changes with the position in the sample (cf. Figs. 1, 2 and refs. [1, 2]). This results in a spatial variation of the diffusion coefficient D_K in the region with columnar solidification.

EXPERIMENTAL PROCEDURE

The experimental set-up was designed to examine the local distribution of the diffusion coefficient in a freeze-drying macroscopic sample and the dependence of the mass transfer properties on the solidification conditions. The solution used in the experiments consists of 10% wt hydroxyethyl starch (HES) in water (for specification of the dry HES powder, cf. refs. [1, 28]). Besides other reasons (cf. ref. [1]), this solution was chosen in order to have the opportunity to compare the results found here with those found in previous experiments with microscopic samples under steady state conditions [1, 2].

Description of the experimental set-up and performance of the experiments

The experimental set-up consists of two main parts:

- the freezing device and
- the freeze-drying set-up.

In the first step of the experiment, the sample is frozen on the freezing device and then, while preventing undesired warming, it is transferred to the freeze-drying device. In both set-ups the same sample container is used.

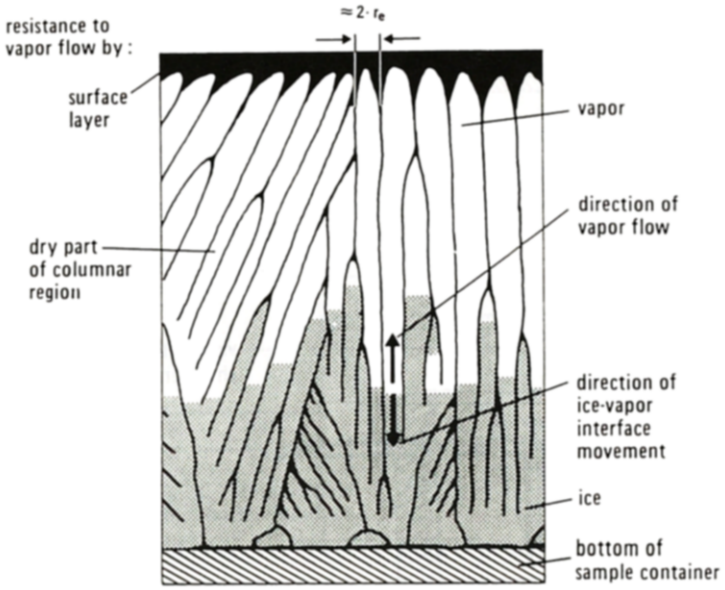

FIG. 2. Sketch explaining the resistances to vapour flow during sublimation.

Sample container

The sample container (Fig. 3) consists of a cylindrical plastic cup with an inner diameter of 40 mm which has a bottom made out of aluminum to ensure a good thermal conductivity and hence a homogeneous temperature of the bottom. The sample cup is equipped with four copper–constantan thermocouples. One is located in the bottom of the sample (T_R), and the others about 1.5 (T_u), 4 (T_m) and 9 mm (T_h) above the bottom, inside the sample.

Freezing device

For the realization of a wide range of freezing conditions in the sample, a simple freezing device was constructed (Fig. 3). A cylindrical cavity in a plastic block forms the cooling chamber. The sample container is mounted with its heat exchanging bottom on the opening of the cooling chamber. Cooled nitrogen gas is circulated through this chamber. Different freezing conditions could be realized by altering the flow rate of the coolant and by this changing the convective heat transfer to the bottom of the sample.

Freeze-drying device

The freeze-drying device (Fig. 4) is based on a commercially available laboratory scale freeze-dryer. It is equipped with an acrylic bell jar and a valve to disconnect the drying and the condenser chamber. The absolute pressure inside the drying chamber is measured using a capacitance manometer with a res-

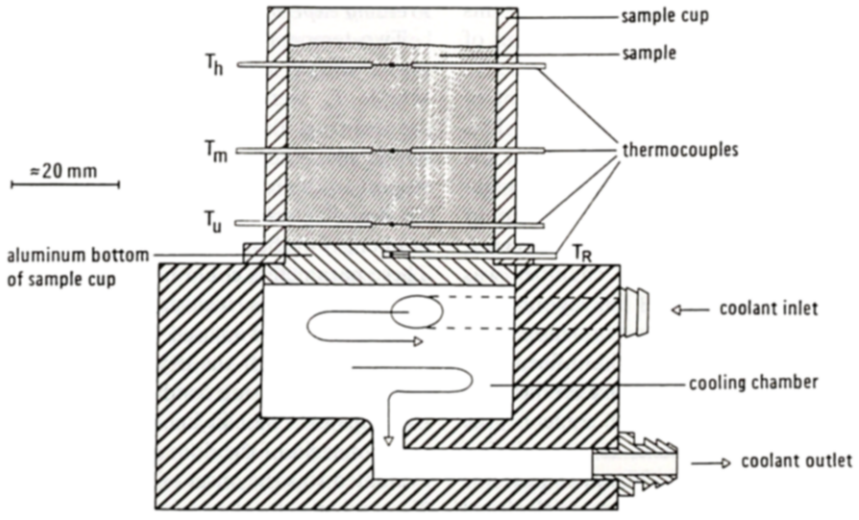

FIG. 3. Sketch of sample container and freezing device (not true to scale). For explanations see text.

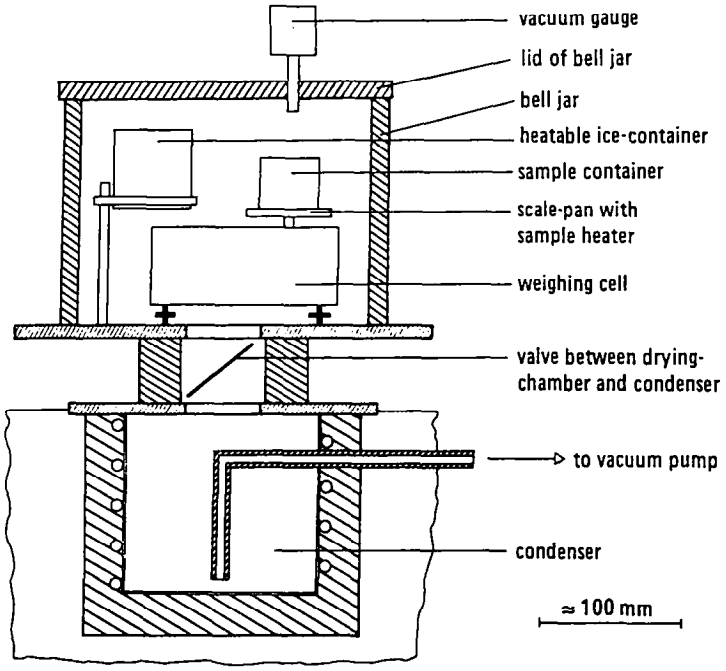

FIG. 4. Sketch of the freeze-drying device (not true to scale). For explanations see text.

olution of 10^{-2} Pa. The mass of the sample is continuously monitored by an electronic balance with a resolution of 1 mg. The balance was modified to fit into the drying chamber and to allow measurements under vacuum conditions. To control the temperature of the sample during sublimation, a spherical aluminum plate with an integrated electrical resistance heater is installed on the scale-pan. The heating power for the electrical sample heater is controlled by means of a two-position controller, built into one of the thermocouple readout instruments. The thermocouple located at the lowest position inside the sample (T_u, Fig. 3) was chosen to measure the actual temperature for the controller. The temperature T_u was kept constant at -20°C (a slight rise of this temperature ($T_{u(max)} = -17$°C) at the later stages of a few of the drying experiments, when the conductive heat flow to the scale-pan exceeded the amount of the heat of sublimation, could not be avoided). This temperature was chosen because it is well below the collapse temperature of -15°C and thus the breakdown of the dry product structure at the ice–vapour interface is avoided (cf. ref. [29]). In most experiments, the absolute pressure in the drying chamber was allowed to attain nearly the value of the vapour pressure in the condenser (≈ 5 Pa at a condenser temperature of ≈ -50°C). To examine the influence of the vapour pressure at the sample surface on the mass transfer properties during drying, in some of the experiments the vapour pressure in the drying chamber was set to a higher value (20 and 40 Pa). For this purpose, a plastic cup with an integrated electrical resistance heater was located in the drying chamber. This cup was filled with distilled water which was frozen and cooled down to about -20°C in a commercial freezer before starting the experiments. The heating power for the heating of this ice block was regulated by means of a two-position controller built into the absolute pressure readout instrument. This kind of vapour pressure control turned out to be very accurate and reliable. For subsequent evaluation, all measured parameters were recorded by means of a microcomputer during the experiments.

EVALUATION OF THE EXPERIMENTS AND RESULTS

Freezing experiments

Two temperatures, the temperature at the bottom of the sample container T_R and in the middle of the sample T_m were recorded during the freezing procedures (Fig. 5). As mentioned above, the parameters which characterize the freezing process best with respect to the resulting ice front morphology are the ice–liquid interface velocity v_{il} and the temperature gradient G at the interface (cf. refs. [1, 2, 15, 16, 18]). These parameters could not be derived directly from the temperatures measured. For this reason, the cooling rate B_R was used as a substitute, in order to plot the results of the drying experiments in dependence of the freezing conditions. B_R is defined here as the slope of a best fit line to the values T_R vs t. The upper margin of the domain where the value of B_R is evaluated was the onset of the freezing process, when T_R reaches a local maximum after the first ice had nucleated in the supercooled solution. The lower mar-

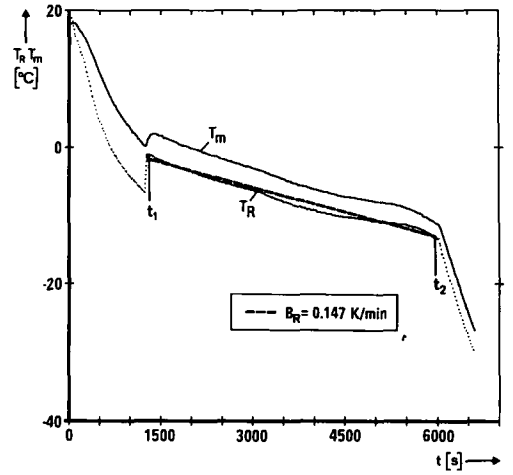

FIG. 5. Recorded temperatures T_R and T_m (cf. Fig. 3), vs time in a freezing experiment, evaluation of the cooling rate B_R.

gin is given by the drop in the temperature–time curve after the first nearly linear temperature decrease (at about -15 to -30°C). The drop is caused by an imposed enhancement of the heat removal at the bottom to reduce the duration of the freezing and cooling process after the ice–liquid interface has reached the surface of the sample.

Sublimation-drying experiments

For a suitable analysis of the drying experiments, the following assumptions were made:

- All heat of sublimation is exchanged through the bottom of the sample container and all heat flow is perpendicular to this bottom. This assumption seems to be justified for the following reasons: for the thin walls of the sample cup (thickness 3.5 mm), a plastic material was chosen which has a very low thermal conductivity (0.14 W m^{-1} K^{-1}) compared to that of the frozen sample ($k_s = 2.19$ W m^{-1} K^{-1}) and that of the aluminum bottom (204 W m^{-1} K^{-1}). The thermal conductivity of the surrounding medium (a vacuum of less than 40 Pa) is negligible. A cover made of aluminum foil (with large openings for unrestricted vapour flow) protects the sample from radiation heat transfer.
- Quasi-steady state conditions were assumed (cf. refs. [1–3]) for the following reasons: the maximum change in sensible heat during the sublimation experiments ($c_{pi} \cdot (T_2 - T_1) = 41$ kJ kg^{-1} with the specific heat of ice c_{pi} (-20°C) = 1.96 kJ kg^{-1} K^{-1} and $T_2 = -15$°C highest and $T_1 = -36$°C lowest temperature measured in the sublimation experiments) is two orders of magnitude smaller than the heat of sublimation (r_s (-26°C) = 2.892×10^3 kJ kg^{-1}, [30]). Additionally, the movement of the ice–vapour interface is very slow (maximum evaluated velocity 1.02 μm s^{-1}). This assumption implies a linear temperature profile in the still frozen part of the sample.
- In spite of the fact that there certainly are small differences in the mass transfer properties of microscopic regions perpendicular to the heat flow direction and thus small lateral perturbations (Figs. 2 and 6), the ice–vapour interface is supposed to propagate as a plane.

The parameters mass of the sample m, pressure in the drying chamber p_∞ and temperatures in the sample at the low, the intermediate and the high position T_u, T_m, T_h are measured as a function of time in the sublimation experiments and used for the analysis.

In the analysis of the sublimation experiments the following values are derived from these parameters as a first step:

the specific mass flux N_v [kg m^{-2} s^{-1}] of vapour through the void fraction of the sample related to the entire cross section A (here 1.26×10^{-3} m^2) of the sample:

$$N_v = \frac{dm}{dt} \cdot \frac{1}{A}. \tag{1}$$

The position of the ice–vapour interface x_{iv} [m]:

$$x_{iv} = \frac{m - m_{tot} \cdot x_{un}}{m_{tot} \cdot (1 - x_{un})} \cdot F. \tag{2}$$

The specific heat flow q through the ice-containing part of the sample [W m^{-2}]:

$$q = N_v \cdot r_s. \tag{3}$$

The temperature at the ice–vapour interface T_{iv} [°C]:

$$T_{iv} = T_u - \frac{q}{k_s} \cdot (x_u - x_{iv}). \tag{4}$$

The water vapour pressure p_{iv} at the interface can be calculated from the temperature T_{iv} by using an approximate relationship p_{iv} [Pa] $= f(T_{iv}$ [K]), [31]:

$$p_{iv} = 133 \cdot 10^{\left(\frac{k_1}{T_{iv}} + k_2 \cdot \log T_{iv} + k_3 \cdot T_{iv} + k_4 \cdot T_{iv}^2 + k_5\right)} \tag{5}$$

with

$$k_1 = -2445.5656, \quad k_2 = 8.2312,$$

$$k_3 = -1677.006 \times 10^{-5},$$

$$k_4 = 120514.0 \times 10^{-10}, \quad k_5 = -6.757169.$$

For every registered data record (time step = 60 s), the values of N_v, x_{iv}, T_{iv} and p_{iv} were calculated using equation (1) (with the differential substituted by a quotient of differences for each pair of successively recorded data of mass and time), and equations (2–5).

Figures 7 and 8 show the time development of the calculated sublimation interface position and the measured and calculated temperatures, respectively. The time-dependent temperatures in Fig. 8 may be explained as follows: at the beginning of the sublimation experiments the frozen sample has a nearly homogeneous temperature of -20°C. During the sublimation experiment the temperature T_u is controlled at that value. First the heat of sublimation

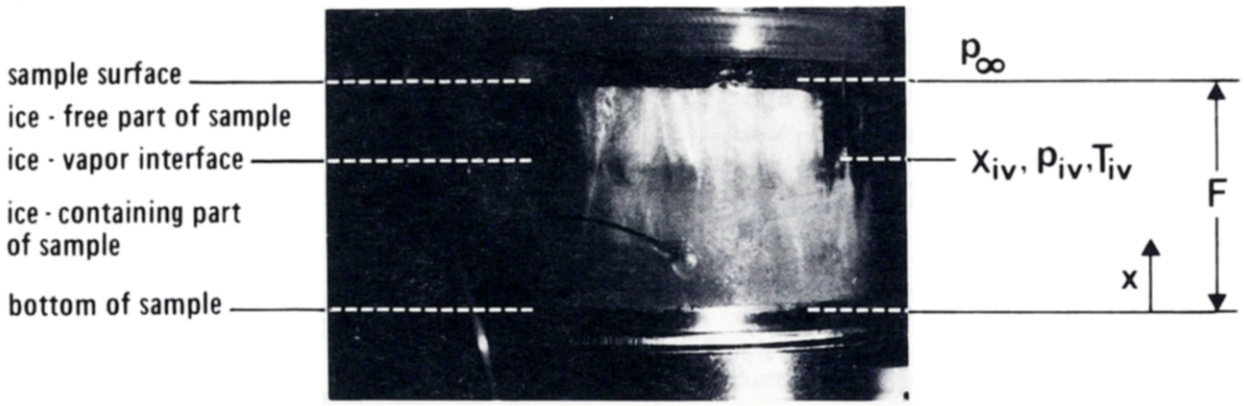

FIG. 6. Photograph of a freeze-drying sample ($F = 18.4$ mm). The sample container is exchanged by a transparent acrylic sample cup and the radiation shelter is removed. The apparent difference in the diameter of the frozen and ice-free part of the sample is an optical artifact caused by the different optical properties at the inner wall of the sample cup with ice or vapour present. No shrinkage of parts of the sample was detectable during the primary drying stage.

is consumed at the surface and there is a heat transfer from the bottom to the surface of the sample. In an initial stage all temperatures except T_u decrease. A quasi-steady state develops with the lowest temperature at the interface and the highest at the bottom. The succeeding increase in the temperatures T_m, T_h and T_{iv} results from a decrease in the rate of sublimation (cf. slope of curve in Fig. 7) and from a decrease in the heat transfer resistance between the bottom and the sublimation interface with the receding interface position.

The consistency of the evaluated values of x_{iv} and T_{iv} with the data directly recorded from the experiments may be checked by comparing the values of T_{iv} with the two temperatures T_m and T_h, recorded in the upper part of the sample at the instances when x_{iv} reaches the two upper thermocouples. Both pressures, p_∞ and p_{iv}, decrease during the initial stage, when the vacuum chamber is evacuated and quasi-steady state conditions are reached. A subsequent increase of p_{iv} results directly from an increase in T_{iv} (cf. Fig. 8 and equation (5)).

Determination of space-dependent diffusion coefficients

The mass flux through the ice-free part of the sample is given by equation (6) for the general case. Applying the ideal gas law, the vapour density can be substituted by the vapour pressure:

$$N_v = -D_e \cdot \frac{d\rho_v}{dx} = -D_e \cdot \frac{1}{R_v \cdot T_{iv}} \cdot \frac{dp_v}{dx}. \qquad (6)$$

The further analysis of the sublimation experiments takes into account that there is a change in texture in the sample and thus a change in resistance to vapour flow as a function of the distance from the heat exchanging bottom. Therefore, effective diffusion coefficients D_{ei} can be calculated, specifically for each layer perpendicular to the mass flow direction (Fig.

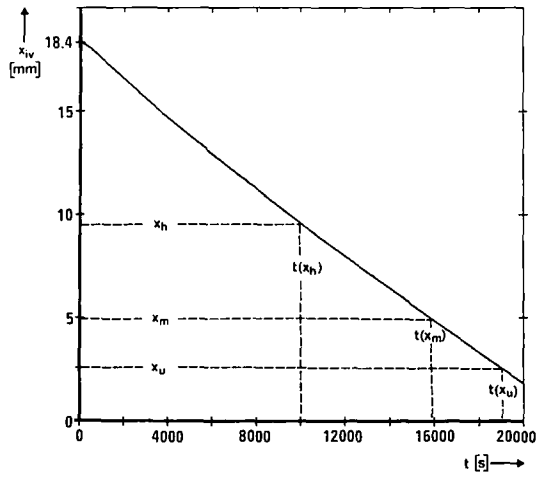

FIG. 7. Calculated sublimation interface position x_{iv} vs time t. $B = 0.147$ K min^{-1}, $T_i = 18.5$°C, $p_\infty \approx 5$ Pa (other parameters constant for all experiments (see text)). The change in interface position x_{iv} is assumed to be proportional to the change in mass m (cf. equation (2)).

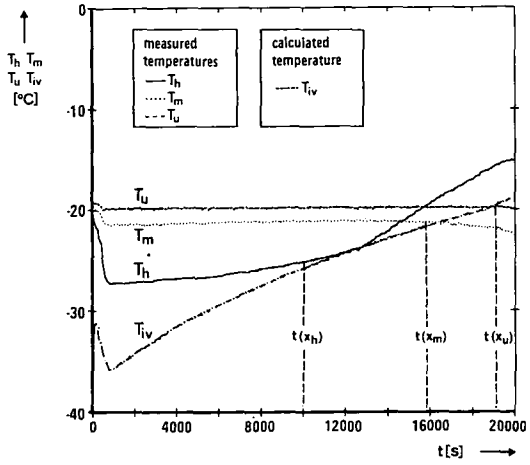

FIG. 8. Temperatures T_u, T_m, T_h, recorded in a drying experiment and calculated sublimation interface temperature T_{iv} vs time. $B = 0.147$ K min^{-1}, $T_i = 18.5$°C, $p_\infty \approx 5$ Pa. The values of $t(x_h)$, $t(x_m)$ and $t(x_u)$ were taken from Fig. 7.

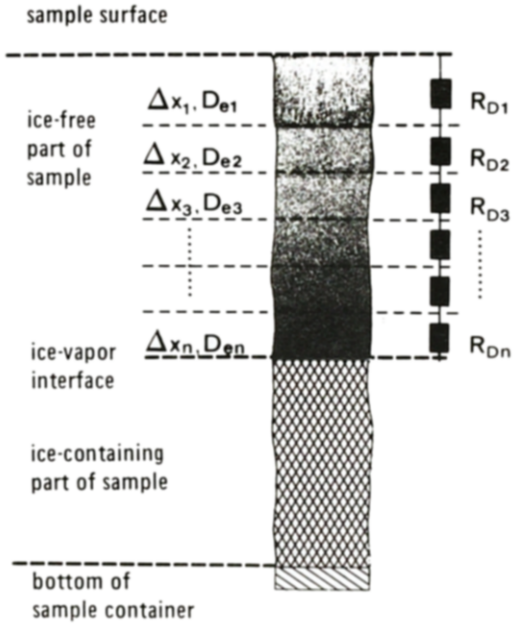

FIG. 9. The 'series of diffusion resistors' model. See text for explanation.

9). A local discretization is performed and thus the differential in equation (6) may be substituted by a quotient of differences:

$$N_v = -D_{ei} \cdot \frac{1}{R_v \cdot T_{iv}} \cdot \frac{\Delta p_{vi}}{\Delta x_i}. \tag{7}$$

A conceptional viewpoint may be introduced here, which is often used in conductive heat transfer problems (cf. ref. [32]) and which uses an analogy to Ohm's law of electrical resistance. The sample is divided into a number of thin layers perpendicular to the direction of mass transfer (Fig. 9). Each layer causes a specific resistance to vapour flow. The resistance R_{Di} corresponds to the thickness of the layer divided by its specific diffusion coefficient ($\Delta x_i/D_{ei}$). As the vapour flow has to pass through all layers in front of the interface, an arrangement of diffusion resistors in series is assumed. The calculated resistance to vapour flow of each layer, corrected for the actual temperature (see below), is assumed to stay constant during the entire sublimation experiment.

In analogy to Ohm's law the overall resistance of the ice-free part of the sample is simply the sum of the resistances of the layers:

$$R_{Dtot} = R_{D1} + R_{D2} + \cdots + R_{Dn}.$$

Applying equation (7) for the n layers in the ice-free part of the sample results in n equations. Equation (8) follows from the simultaneous solution of these equations, assuming continuity of mass flow (as a result of quasi-steady state):

$$N_v = \frac{p_{iv} - p_\infty}{R_v \cdot T \cdot \sum_{i=1}^{n} \frac{\Delta x_i}{D_{ei}}}. \tag{8}$$

This equation, rearranged for the diffusion coefficient D_{en} of the layer right in front of the interface yields:

$$D_{en} = \frac{\Delta x_n}{\frac{p_{iv} - p_\infty}{N_v \cdot R_v \cdot T_{iv}} - \sum_{i=1}^{n-1} \frac{\Delta x_i}{D_{ei}}}. \tag{9}$$

For each experiment, equation (9) could be solved successively for the different layers of the sample (Fig. 9). Equation (9) was calculated m times (beginning with layer 1) for the m layers of a sample. For clarity the following example is given.

The position of the interface attains the value of the lower boundary of the layer under consideration ($x_{iv} = x_{ivn}$). Then, the diffusion coefficient D_{en}, specific for the layer n could be calculated with the values of N_v, p_{iv}, p_∞ and T_{iv} at the time $t(x_{iv} = x_{ivn})$ and with the sum of the previously calculated resistances $\Delta x_i/D_{ei}$ of the layers above of the layer n (corrected for the actual value of T_{iv}).

The temperature correction was performed under the assumption that mass transfer is mainly effected by Knudsen flow (cf. refs. [1, 2, 5]), and with the functional dependence $D_e \sim \sqrt{T}$ (cf. refs. [1, 27]). The diffusion coefficients D_e to be given below are corrected for a reference temperature of $-20°C$.

$$D_e = D_e(T_{iv}) \cdot \frac{\sqrt{(253.15\,K)}}{\sqrt{(T_{iv})}}. \tag{10}$$

Results of the experiments

Figure 10 shows a typical spatial distribution of vapour diffusion coefficients D_e (i.e. the temperature ($-20°C$) corrected values of D_{en} plotted at the positions of the respective layers) in a freeze-drying sample. The evaluation of the experiments according to the above described procedure and the representation of the results as diffusion coefficients for each distinct layer of the sample is a superior basis to discuss the influence of the freezing process on the

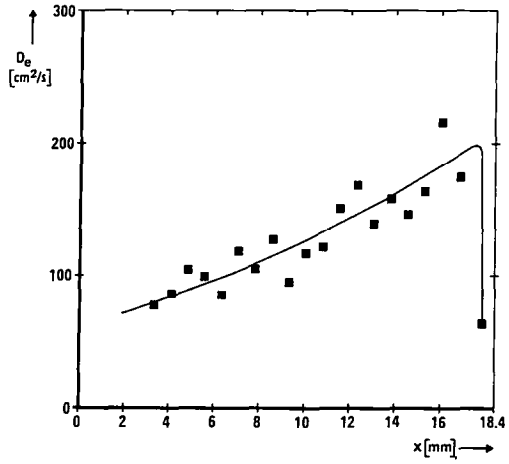

FIG. 10. Typical local distribution of the effective diffusion coefficient D_e in a freeze-drying sample (line fitted by eye). $B = 0.147$ K min^{-1}, $T_i = 18.5°C$, $p_\infty = 5$ Pa.

sublimation step as compared to the evaluation of an overall mass transfer coefficient for the dry layer of a freeze-drying sample (cf. refs. [5, 9]). The layers of the sample close to the heat exchanging bottom (solidification had started in this part of the sample during the freezing step) yield small values of the diffusion coefficient D_e. The value of D_e increases with the distance from the bottom, reaching a maximum value in the layers of the sample close to the surface. The surface layer forms a decisive barrier against vapour transport, and thus exhibits a very small value of D_e.

This characteristic profile of diffusion coefficients is shifted to higher values if the cooling rate B_R is decreased (cf. Fig. 11). The diffusion coefficient D_e of the surface layer seems to show an exception to this rule. In this surface layer no significant change of the diffusion coefficient D_e is detectable at different freezing conditions.

The process of desorption, i.e. the removal of unfrozen water 'bound' to the solutes, may already start in the upper parts of the sample where the vapour pressure is very low, when ice is still present in the lower parts of the sample. In order to estimate whether the process of desorption has an influence on the mass transfer coefficient D_e in the sample, some experiments were performed with similar cooling rates, but with different vapour pressures p_∞ in the vacuum chamber during sublimation. With increasing p_∞, the diffusion coefficients seem to be shifted to slightly lower values, but this trend is not very pronounced and significant.

Besides the cooling rate B_R applied to the bottom of the sample, the initial temperature T_i of the sample at the beginning of the freezing process could be varied to alter the solidification conditions. To determine the influence of this parameter, experiments were performed with the temperature T_i changed from room temperature ($T_i = 20 \pm 2°C$) to $T_i = 1 \pm 1°C$. With different initial temperatures T_i and similar cooling rates B_R, no distinct change in mass transfer properties could be detected in our experiments (Fig. 12).

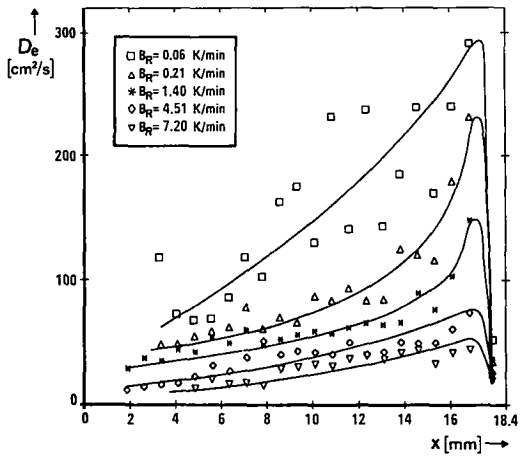

FIG. 11. Local distribution of the effective diffusion coefficient D_e in freeze-drying samples for different cooling rates B_R during solidification (curves fitted by eye). $T_i \approx 20 \pm 2°C$, $p_\infty = 5$ Pa.

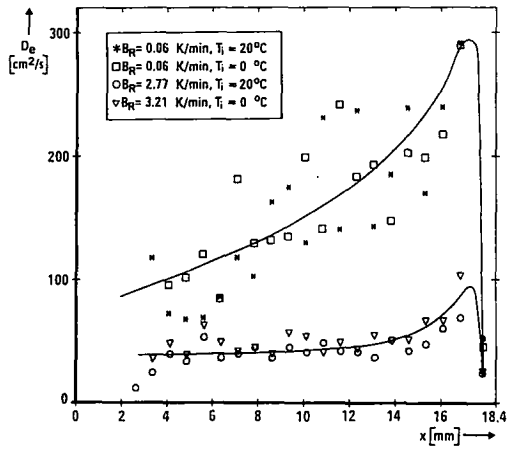

FIG. 12. Local distribution of the effective diffusion coefficient for similar cooling rates B_R but different initial temperatures T_i at the beginning of the freezing procedure (curves fitted by eye). $p_\infty = 5$ Pa.

DISCUSSION AND CONCLUSIONS

It could be seen that the value of the diffusion coefficient for vapour transport out of the freeze-drying sample strongly depends on the position in the macroscopic specimen (Fig. 10). Furthermore, the diffusion coefficient is significantly influenced by the cooling conditions imposed onto the sample (Fig. 11). This behaviour of the diffusion coefficient may be largely attributed to differences in the freezing conditions, determining the morphology of the solid–liquid interface and the inner texture of the sample after complete freezing (cf. refs. [1, 2, 33]). When trying to compare the results found here with those of previously reported measurements under steady state conditions [1], it has to be taken into account that in a macroscopic sample dynamic freezing occurs. Thus, the solidification conditions at the interface (ice–liquid interface velocity v_{il} and temperature gradient G) vary with time and may not instantaneously result in a primary spacing λ_1 according to the steady state value. But it is generally accepted that there is a temporal development of the value of λ_1 towards the stationary situation (cf. refs. [18–20]). It remains unclear, however, which of the following superposed mechanisms during the dynamic freezing process in a macroscopic sample controls the solidification texture: the dynamic development of a columnar interface from the initially formed equiaxed crystals, the dynamic change of the columnar morphology towards the steady state value of λ_1, or the adjustment of λ_1 due to the continuous change of the values of the parameters v_{il} and G at the ice–liquid interface. For a given initial temperature T_i a decrease in the cooling rate B_R always corresponds to a decrease in the parameters v_{il} and/or G. A significant shift of the diffusion

coefficient in the different layers of the sample to higher values for a decrease of B_R could be observed in the reported experiments (Fig. 11). Consequently this may be attributed to a higher average value of λ_1 (caused by lower values of v_{il} and G). A higher value of λ_1 implies a larger value of the average radius r_e of the void channels used as passageways for vapour transport during the drying process (cf. equation (3)). As an exception to this cooling rate dependence, the resistance to vapour flow by the surface layer is nearly independent of the bottom cooling rate B_R (Fig. 11).

The diffusion coefficients measured here ($10 \leqslant D_e \leqslant 300$ cm^2 s^{-1}) are comparable to the values measured in corresponding steady state experiments ($10 \leqslant D \leqslant 100$ cm^2 s^{-1}) (cf. refs. [1, 2]). For a more detailed comparison of both investigations, the spatial variation of the parameters v_{il} and G has to be evaluated separately for the freezing conditions imposed to macroscopic samples. This may be performed by numerical modelling of the freezing processes applied in this investigation (cf. refs. [14, 23, 34, 35]).

Other investigations on the freeze-drying process often report a nearly constant mass-flow out of the sample during primary drying [9, 10, 36, 37]. This could be observed in our experiments as well (Fig. 7). As proposed by Quast and Karel [9], this is partially a result of the decisive influence of the mass transfer resistance of the surface layer of the sample (Figs. 10 and 11).

Studies of the mathematical modelling of the freeze-drying process, in most cases assume a constant diffusion coefficient throughout the whole sample (e.g. refs. [11, 38–40]). This practice should certainly be avoided, as the results presented in this publication show differences in the diffusion coefficient of up to about 425% in the different layers of the sample.

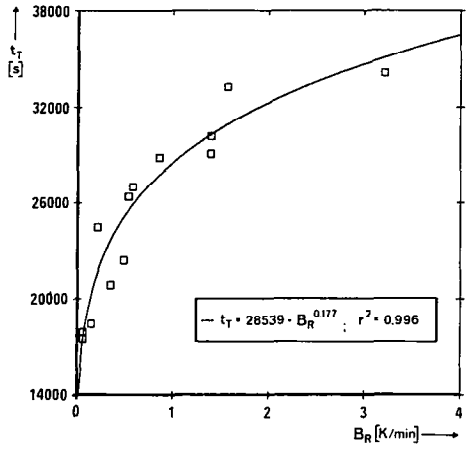

FIG. 13. Drying time t_T for obtaining a residual ice content of 3.13 g in the above described drying experiments vs the cooling rate B_R, i.e. the duration to sublime 16 g of the ice initially present in the sample. Up to a residual ice content of 3.13 g, a temperature T_u of -20 ± 0.3°C and thus comparable conditions could be controlled in the experiments evaluated for the t_T values. $T_i = 20 \pm 2$°C, $p_\infty = 5$ Pa.

The practical relevance of the shown investigations may be demonstrated by differences in drying time t_T. Figure 13 shows drying times at different cooling rates B_R. It may be seen, that depending on the chosen cooling rate B_R, the drying time may be reduced to a half.

Acknowledgement—The authors would like to thank the students Bernhard Reul, Detlef Zander and Armin Huck for their helpful assistance.

REFERENCES

1. M. Kochs, C. Körber, B. Nunner and I. Heschel, The influence of the freezing process on vapour transport during sublimation in vacuum-freeze-drying, *Int. J. Heat Mass Transfer* **34**, 2395–2408 (1991).
2. M. Kochs, Die Bedeutung des Friervorganges bei der Gefriertrocknung, Doctoral Dissertation, Fak. Maschinenwesen, RWTH Aachen (1991).
3. N. F. Ho and T. J. Roseman, Lyophilization of pharmaceutical injections: theoretical physical model, *J. Pharm. Sci. (J. Am. pharm. Ass.)* **68**, 1170–1174 (1979).
4. M. J. Pikal, S. Shah, D. Senior and J. E. Lang, Physical chemistry of freeze-drying: measurement of sublimation rates for frozen aqueous solutions by a microbalance technique, *J. Pharm. Sci. (J. Am. pharm. Ass.)* **72**, 635–650 (1983).
5. W. E. Spieß, Über den Transport des Wasserdampfes bei der Gefriertrocknung von Lebensmitteln, Doctoral Dissertation, Fak. Maschinenwesen, TH Karlsruhe (1969).
6. J. D. Mellor, *Fundamentals of Freeze-Drying*. Academic Press, New York (1978).
7. P. Mazur and J. J. Schmidt, Interaction of cooling velocity, temperature, and warming velocity on the survival of frozen and thawed yeast, *Cryobiology* **5**, 1–17 (1968).
8. T. Nei, T. Araki and H. Souzu, Studies of the effect of drying conditions on residual moisture content and viability in the freeze-drying of microorganisms, *Cryobiology* **2**, 68–73 (1965).
9. D. G. Quast and M. Karel, Dry layer permeability and freeze-drying rates in concentrated fluid systems, *J. Food Sci.* **33**, 70–175 (1968).
10. K. Nakamura, H. Kumagai and T. Yano, Effect of freezing conditions on freeze drying rate of concentrated liquid foods, *Food Eng. Process Appl. Transp. Phenom.* **1**, 445–450 (1986).
11. D. F. Dyer and J. E. Sunderland, Bulk and diffusional transport in the region between molecular and viscous flow, *Int. J. Heat Mass Transfer* **9**, 519–526 (1966).
12. J. D. Mellor, Vapour transfer problems in the course of freeze-drying. In *Advances in Freeze-Drying* (Edited by L. Rey), pp. 75–88. Hermann, Paris (1966).
13. D. MacFarlane, Devitrification in glass-forming aqueous solutions, *Cryobiology* **23**, 230–244 (1986).
14. U. Hartmann, Wärmetechnische Aspekte des Gefrierens bei der Kryokonservierung lebender Zellen, Doctoral Dissertation, Fak. Maschinenwesen, RWTH Aachen (1987).
15. W. Kurz and D. Fisher, *Fundamentals of Solidification* (3rd Edn). Trans. Tech. Publications, Aedermannsdorf/Switzerland (1989).
16. J. D. Hunt, Cellular and primary dendrite spacings. In *Solidification and Casting of Metals*, Proceedings of an international conference on solidification, Sheffield, England 1979, published by The Metals Society, 3–9 (1979).

17. W. Kurz and D. J. Fisher, Dendrite growth at the limit of stability: tip radius and spacing, *Acta metall.* **29,** 11–20 (1981).
18. R. Trivedi and K. Somboonsuk, Pattern formation during the directional solidification of binary systems, *Acta metall.* **33,** 1061–1068 (1985).
19. K. Somboonsuk and R. Trivedi, Dynamic studies of dendritic growth, *Acta metall.* **33,** 1051–1060 (1985).
20. V. Seetharaman, M. A. Eshelman and R. Trivedi, Cellular spacing—II. Dynamic studies, *Acta metall.* **36,** 1175–1185 (1988).
21. B. Nunner, Ch. Körber, G. Rau, A. Hubel and E. G. Cravalho, Characterization of phase front morphologies in aqueous solutions subjected to directional solidification, *Cryobiology* **26,** 559 (1989).
22. M. Kochs, P. Schwindke and C. Körber, A microscope stage for the dynamic observation of freezing and freeze-drying in solutes and cell suspension, *Cryo-Letters* **12,** 401–419 (1989).
23. M. Jochem, U. Hartmann and Ch. Körber, Modelling of coupled heat and mass transfer problem of nonplanar solidification and melting in aqueous solutions and numerical treatment. In *Network Thermodynamics, Heat and Mass Transfer in Biotechnology* (Edited by K. R. Diller), pp. 73–80. American Society of Mechanical Engineers, New York (1987).
24. M. C. Flemings, *Solidification Processing.* McGraw-Hill, New York (1974).
25. M. Jochem, Erwärmen und Schmelzen wäßriger Lösungen bei der Gefrierkonservierung von Zellen, Doctoral Dissertation, Fak. Maschinenwesen, RWTH Aachen (1989).
26. T. Nei, Formation of cracks in the freezing and freeze-drying of some biological preparations, *Biodynamics* **9,** 247–255 (1964).
27. C. N. Satterfield, *Mass Transfer in Heterogeneous Catalysis.* M.I.T. Press, Cambridge, Massachusetts (1970).
28. A. Sputtek, Hydroxyethylstärke: Synthese, Eigenschaften und Anwendung als Schutzadditiv in der Kryobiologie, Doctoral Dissertation, Fak. Medizin RWTH Aachen (1990).
29. A. P. MacKenzie, Collapse during freeze-drying—qualitative and quantitative aspects. In *Freeze Drying and Advanced Food Technology* (Edited by S. A. Goldblith, L. Rey and W. W. Rothmayr), pp. 277–307. Academic Press, New York (1975).
30. Z. D. Zwetkow, *Vakuumgefriertrocknung.* VEB Fachbuchverlag, Leipzig, Germany (1977).
31. E. H. Kennard, *Kinetic Theory of Gases.* McGraw-Hill, New York, London (1938).
32. J. P. Holman, *Heat Transfer.* McGraw-Hill, New York (1981).
33. B. Nunner, Characterization of the ice front morphology developing during directional solidification of aqueous solutions, to be submitted to *J. Chrystal Growth.*
34. U. Hartmann, B. Nunner, Ch. Körber and G. Rau, Where should the cooling rate be determined in an extended freezing sample? *Cryobiology* **27,** 279–287 (1990).
35. M. Jochem and Ch. Körber, Numerical solution of the coupled heat and mass transfer problem of non-planar solidification and melting in aqueous solutions, *Wärme- und Stoffübertragung* (submitted).
36. J. B., Lambert and W. R. Marshall, *Freeze-Drying of Foods*, pp. 105–133. Proc. Natl. Acad. Sci., Nat. Res. Council (1962).
37. R. F. Burke and R. V. Decareau, Recent advances in the freeze-drying of food products, *Adv. Food Res.* **13,** 1–89 (1964).
38. D. F. Dyer and J. E. Sunderland, Heat and mass transfer mechanisms in sublimation dehydration, *J. Heat Trans.* **90,** 379–384 (1968).
39. S. Lin, An exact solution of the sublimation problem in a porous medium, *J. Heat Trans.* **103,** 165–168 (1981).
40. S. Lin, An exact solution of the sublimation problem in a porous medium, Part II—With an unknown temperature and vapour concentration at the moving sublimation front, *J. Heat Trans.* **104,** 808–811 (1982).
41. M. Jochem and Ch. Körber, Extended phase diagrams for the ternary solutions H_2O–NaCl–glycerol and H_2O–NaCl–hydroxyethylstarch (HES) determined by DSC, *Cryobiology* **24,** 513–536 (1987).
42. Ch. Körber, Phenomena at the advancing ice–liquid interface: solutes, particles and biological cells, *Quart. Rev. Biophys.* **21,** 229–298 (1988).